

1 Revealing Free Energy Landscape from MD Data via Conditional
2 Angle Partition Tree
3 Supplementary Material

4 Hangjin Jiang¹, Xuhui Huang², Han Li³, Wing Hung Wong^{4*}, Xiaodan Fan^{5*}

1¹Center for Data Science, Zhejiang University

2²Department of Chemistry, The Hong Kong University of Science and Technology

3³College of Economics, Shenzhen University

4⁴Department of Statistics, Stanford University

5⁵Department of Statistics, The Chinese University of Hong Kong

5 **1 Overview of MD data and transition matrix**

6 Figure 1 shows an overview of MD trajectory data and related transition matrix in two-step clustering
7 procedure.

8 **2 Data Preparation**

9 The input of CAPT is a set of MD trajectories. We use the R package 'bio3d' [1] to get all torsion angles of
10 all frames of the MD trajectories. In this paper, we only use the backbone torsion angles, i.e., ϕ 's and ψ 's.

11 **3 Details about analyzing Alanine dipeptide**

12 **3.1 Visualization of Alanine dipeptide data**

13 Figure 2 shows the histograms of angles (ψ, ϕ) of Alanine dipeptide. Figure 3 shows the distribution of the
14 frames of Alanine dipeptide data in the angle phase.

15

16

17 **3.2 Settings for PCCA, PCCA+, MPP and Gibbs**

18 When using PCCA/PCCA+, one should specify the range of the number of clusters, i.e., the maximal number
19 of clusters n_{max} and minimal number of clusters n_{min} . We set $n_{max} = n_{min} = 6$ for PCCA, and $n_{max} = 9$
20 and $n_{min} = 3$ for PCCA+. The Gibbs sampling algorithm is also run with the true number of clusters.

21 To use PCCA, PCCA+, MPP and Gibbs sampling method, one has to cluster frames into microstates first.
22 In the simple case of Alanine dipeptide which only has two torsion angles, we use a grid method in the angle
23 space to group frames to microstates. More specifically, we partition the whole space $[-\pi, \pi] \times [-\pi, \pi]$ into

*Corresponding Author: whwong@stanford.edu and xfan@cuhk.edu.hk

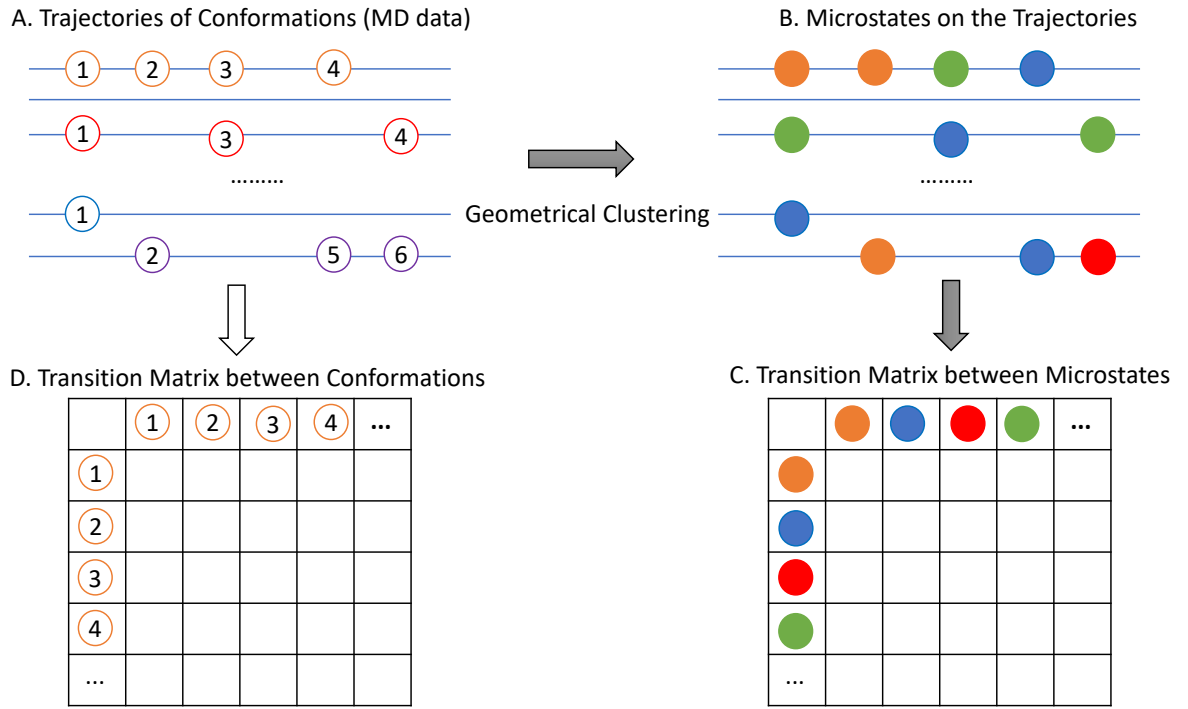


Figure 1: MD trajectory data and related transition matrix. (A) shows the trajectories of conformations (denoted by empty circles) obtained from molecular dynamics simulation. Note that circles in different color denote different conformations in different trajectories. (B) shows the trajectories of microstates (denoted by solid colored circles) by mapping conformations to microstates through geometrical clustering. (C) shows the transition matrix, $T(m \times m)$, between microstates obtained from trajectories of conformations in sub-figure (B), where m , usually no more than thousands, is the number of microstates obtained by geometrical clustering in the splitting step. The entry of this matrix, T_{ij} , is the number of jumping from microstate i to microstate j along the trajectories. That is, T_{ij} is the number of times we observe in all trajectories that the microstate i is followed by microstate j . (D) shows the transition matrix, $K(n \times n)$, between conformations obtained from trajectories of conformations in sub-figure (A), where n , usually at the magnitude of millions, is the number of conformations observed in MD simulations. The entry of this matrix, K_{ij} , is the counts of jumping from conformation i to conformation j along the trajectories. That is, K_{ij} is the number of times we observe in all trajectories that the conformation i is followed by conformation j . Since any two conformations along the trajectories are different, $L(s - 1)$ of the entries of K are 1, and others are 0, thus non-informative for detecting stable structures, where L is the number of trajectories, s is the number of conformations in each trajectory, and $n = L \times s$.

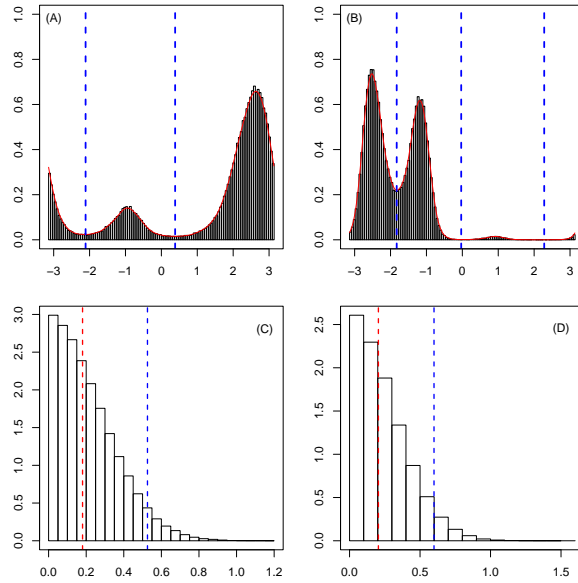


Figure 2: Histograms of angles (ψ, ϕ) of Alanine dipeptide. (A) and (B) are the histograms of ψ and ϕ , respectively. (C) and (D) are the histograms of the one-step distance of ψ and ϕ , respectively. In (A) and (B), the blue dashed lines show the partition positions found by CAPT. In (C) and (D), the blue and red dashed lines correspond to the 95% and 50% quantiles of the distribution, respectively.

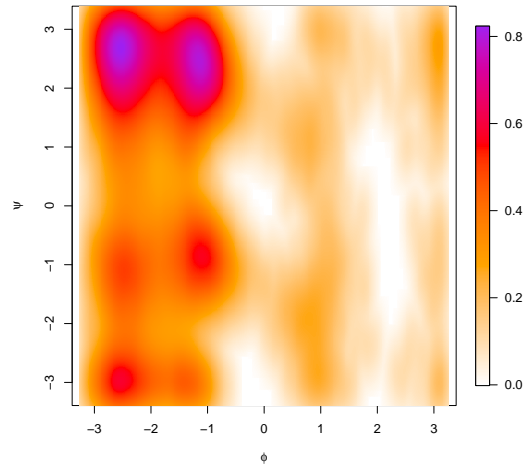


Figure 3: Scatter plot of frames of Alanine dipeptide data in the angle phase. The Alanine dipeptide is a small biomolecule with only two torsion angles, say, ϕ and ψ , and its free energy landscape is fully determined by these two angles.

²⁴ a 80×80 grid, and take each small grid as a microstate. The center of each small grid cell is treated as the
²⁵ center of this microstate. In fact, by dividing the (ϕ, ψ) space into 6400 bins, we get many empty bins and
²⁶ remove them from our analysis. We take each non-empty bin as a microstate, and map each conformation
²⁷ in the trajectory to the corresponding microstate, then we get trajectories of microstates, and the transition
²⁸ matrix between microstates.

²⁹ 3.3 Transition matrix from different methods

³⁰ Table 1 shows the transition matrix of the benchmark clusters of Alanine dipeptide, Table 2 shows results
³¹ from CAPT, Table 4 shows results from PCCA, Table 3 shows that of clusters of Alanine dipeptide obtained
by MPP, Table 5 show results from PCCA+, Table 6 show results from Gibbs sampling method.

Table 1: Transition matrix of the benchmark clusters of Alanine dipeptide

	S1	S2	S3	S4	S5	S6
S1	0.9457	0.0477	0.0062	0.0004	0.0000	0.0000
S2	0.0609	0.9365	0.0004	0.0021	0.0000	0.0002
S3	0.0403	0.0021	0.8939	0.0636	0.0000	0.0000
S4	0.0020	0.0090	0.0526	0.9356	0.0008	0.0000
S5	0.0013	0.0013	0.0000	0.0098	0.9718	0.0158
S6	0.0000	0.0401	0.0000	0.0000	0.0519	0.9080
Sum of diagonals: 5.591479						
Mean of diagonals: 0.9319131						
Minimal of diagonals: 0.8939						

³²

Table 2: Transition matrix between clusters of Alanine dipeptide obtained by CAPT

	S011	S012	S013	S021	S022	S023
S011	0.9461	0.0475	0.0000	0.0061	0.0003	0.0000
S012	0.0613	0.9360	0.0002	0.0004	0.0021	0.0000
S013	0.0027	0.0163	0.9074	0.0000	0.0000	0.0736
S021	0.0407	0.0019	0.0000	0.8932	0.0642	0.0000
S022	0.0018	0.0095	0.0000	0.0515	0.9364	0.0009
S023	0.0000	0.0000	0.0975	0.0000	0.0176	0.8848
Sum of diagonals: 5.50389						
Mean of diagonals: 0.917315						
Minimal of diagonals: 0.8848						

Table 3: Transition matrix between clusters of Alanine dipeptide obtained by MPP

	S0	S1	S2	S3	S4	S5
S0	0.0526	0.3289	0.0000	0.1447	0.4342	0.0395
S1	0.0013	0.8124	0.0001	0.0460	0.1391	0.0011
S2	0.0000	0.2778	0.0556	0.6667	0.0000	0.0000
S3	0.0001	0.0159	0.0002	0.8503	0.1335	0.0000
S4	0.0003	0.0330	0.0000	0.0918	0.8745	0.0005
S5	0.0241	0.3012	0.0000	0.0361	0.6145	0.0241
Sum of diagonals: 2.669393						
Mean of diagonals: 0.4448989						
Minimal of diagonals: 0.0241						

Table 4: Transition matrix between clusters of Alanine dipeptide obtained by PCCA

	S1	S2	S3	S4	S5	S6
S1	0.9352	0.0003	0.0018	0.0000	0.0000	0.0626
S2	0.0477	0.9131	0.0000	0.0068	0.0324	0.0000
S3	0.0042	0.0000	0.9752	0.0000	0.0004	0.0202
S4	0.0000	0.0032	0.0000	0.9104	0.0816	0.0048
S5	0.0000	0.0269	0.0175	0.0672	0.8884	0.0000
S6	0.0508	0.0000	0.0068	0.0000	0.0000	0.9424
Sum of diagonals: 5.564797						
Mean of diagonals: 0.9274662						
Minimal of diagonals: 0.8884						

Table 5: Transition matrix between clusters of Alanine dipeptide obtained by PCCA+

	S1	S2	S3	S4	S5	S6	S7	S8	S9
S1	0.7667	0.1333	0.0000	0.1000	0.0000	0.0000	0.0000	0.0000	0.0000
S2	0.0096	0.9349	0.0096	0.0145	0.0000	0.0000	0.0000	0.0000	0.0313
S3	0.0000	0.0045	0.8649	0.1194	0.0000	0.0000	0.0000	0.0068	0.0045
S4	0.0030	0.0089	0.0523	0.9211	0.0000	0.0148	0.0000	0.0000	0.0000
S5	0.0000	0.0000	0.0000	0.0000	0.6736	0.0412	0.0659	0.1643	0.0550
S6	0.0000	0.0000	0.0000	0.0009	0.0069	0.9344	0.0539	0.0003	0.0037
S7	0.0000	0.0000	0.0000	0.0000	0.0144	0.0596	0.8945	0.0296	0.0019
S8	0.0000	0.0000	0.0000	0.0000	0.0052	0.0000	0.0046	0.9419	0.0483
S9	0.0000	0.0001	0.0000	0.0000	0.0022	0.0009	0.0005	0.0601	0.9361
Sum of diagonals: 7.86813									
Mean of diagonals: 0.8742366									
Minimal of diagonals: 0.6736									

3.4 Discussion

If we compare the energy landscape of benchmark clusters of Alanine dipeptide with that obtained by CAPT, although ARI is as high as 0.987002, we can still find a small difference: the boundary between S013 and S023 in Figure 4(B) is a bit higher than that between S5 and S6 in Figure 4(A). This small difference is due to the order of angles used for partitioning. Table 7 gives the transition matrix when using different angles in the first step of CAPT for Alanine dipeptide. The ψ column is the transition matrix between clusters obtained by partitioning all frames into 2 clusters according to the distribution of ψ , where the partition score is 0.9728. The ϕ column is the transition matrix between clusters obtained by partitioning all frames into 3 clusters according to the distribution of ϕ , where the partition score is 0.9395. Thus CAPT prefers using ψ to partition in the first step. That means that CAPT is a bit greedy in transition probability, which leads to the small discrepancy from the benchmark.

Alternatively, if CAPT had used ϕ first in constructing the partition tree, we would get the energy landscape as shown in Figure 4, which would be closer to the benchmark in Figure 4(A) (ARI=0.9873). The corresponding transition matrix is given in Table 8. This implies that there is room to improve the performance of CAPT if we can find a more suitable partition score.

48

3.5 Sensitivity Analysis

As we can see from the results of PCCA+ in Figure 4, PCCA+ overestimates the number of clusters under the setting in Section 2.2 of this Supplementary Material. We try another setting for PCCA+, $n_{max} = 5$ and

Table 6: Transition matrix between clusters of Alanine dipeptide obtained by Gibbs Sampling method

	S0	S1	S2	S3	S4	S5
S0	0.9349	0.0012	0.0018	0.0605	0.0001	0.0015
S1	0.0058	0.8783	0.0666	0.0443	0.0002	0.0047
S2	0.0073	0.0562	0.9313	0.0029	0.0010	0.0013
S3	0.0477	0.0069	0.0007	0.9429	0.0000	0.0018
S4	0.0033	0.0020	0.0113	0.0020	0.9515	0.0299
S5	0.1374	0.0640	0.0284	0.1919	0.0509	0.5273
Sum of diagonals: 5.1662						
Mean of diagonals: 0.8610						
Minimal of diagonals: 0.5273						

Table 7: Transition matrix when using different partition schemes in the first step

ψ		ϕ				
		S1	S2	S3		
S1	0.9949	0.0051	S1	0.9496	0.0503	0.0000
S2	0.0272	0.9728	S2	0.0602	0.9395	0.0003
-	-	-	S3	0.0015	0.0174	0.9811

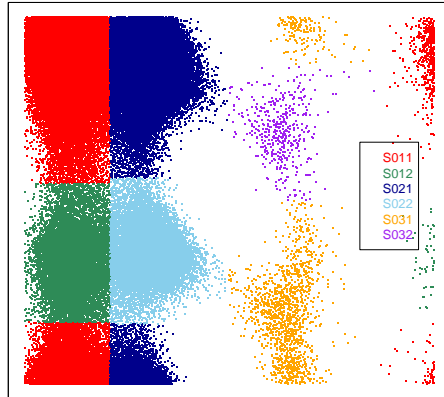


Figure 4: Energy landscape of Alanine dipeptide obtained from CAPT by using firstly ϕ to partition the angle space.

52 $n_{min} = 7$, denoted as PCCA+'. We also run the Gibbs sampling algorithm with 5 and 7 clusters, denoted by
53 Gibbs' and Gibbs''. Transition matrices from PCCA+', Gibbs' and Gibbs'' are shown in Table 9, Table 10
54 and Table 11. The clustering results are shown in Figure 5. All these results show that both PCCA+ and
55 Gibbs sampling algorithm depend strongly on the pre-selected number of clusters. However, the number of
56 stable states (clusters) is usually unknown to us and it is the key quantity to be estimated from the data.

57

58 As reported in [2–4], Dihedral PCA gives clear energy landscape of biomolecules. However, while we try it on
59 Alanine dipeptide, its partitioning is not clear as shown in Figure 6.

60

61 For sensitivity analysis of our algorithm, we check the effect of parameters P_0 and S_0 as well as the kernel
62 function while applying CAPT on Alanine dipeptide MD data. For the kernel function, we tried different

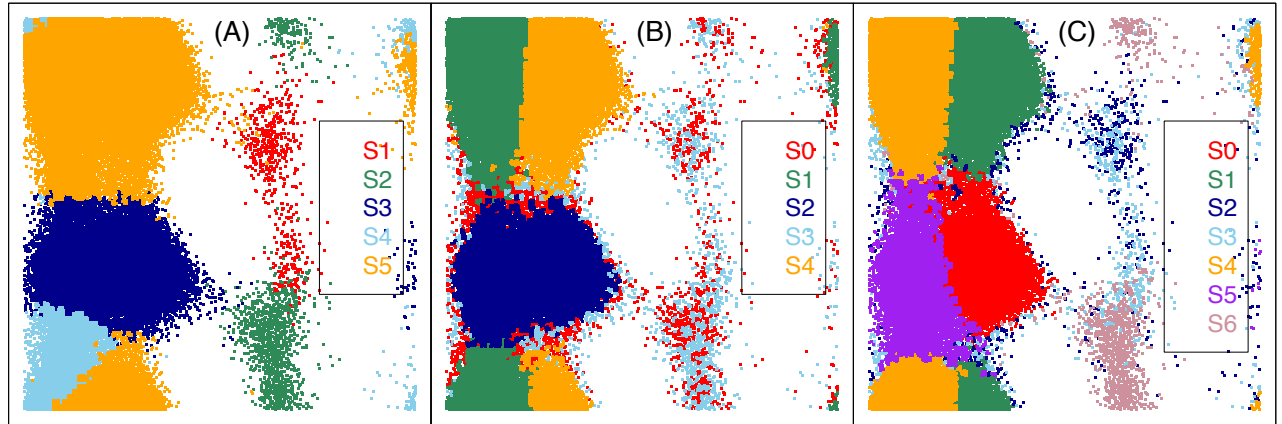


Figure 5: Clustering result of Alanine dipeptide from PCCA+['] (A), Gibbs' (B) and Gibbs'' (C).

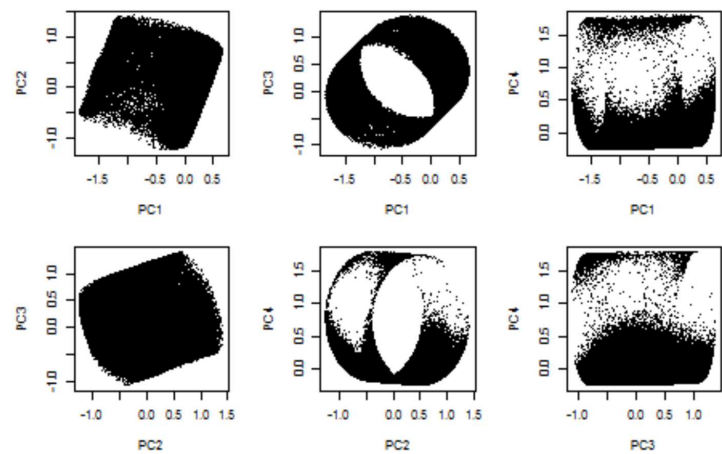


Figure 6: The effect of Dihedral PCA on Alanine dipeptide. We apply Dihedral PCA to the Alanine dipeptide data, but do not see any pattern explored by PCA.

Table 8: Transition matrix between clusters when first using ϕ to partition in CAPT

	S011	S012	S021	S022	S031	S032
S011	0.9459	0.0060	0.0476	0.0005	0.0000	0.0000
S012	0.0415	0.8920	0.0017	0.0647	0.0000	0.0000
S021	0.0614	0.0003	0.9361	0.0021	0.0000	0.0002
S022	0.0021	0.0517	0.0095	0.9357	0.0009	0.0000
S031	0.0007	0.0000	0.0000	0.0106	0.9774	0.0113
S032	0.0045	0.0000	0.0403	0.0000	0.0336	0.9217
Sum of diagonals: 5.608926						
Mean of diagonals: 0.934821						
Minimal of diagonals: 0.8920						

Table 9: Transition matrix between clusters of Alanine dipeptide obtained by PCCA+'

	S1	S2	S3	S4	S5
S1	0.9049	0.0616	0.0000	0.0000	0.0335
S2	0.0257	0.9592	0.0113	0.0008	0.0030
S3	0.0000	0.0005	0.9591	0.0257	0.0147
S4	0.0000	0.0001	0.0668	0.5796	0.3535
S5	0.0001	0.0000	0.0025	0.0241	0.9732
Sum of diagonals: 4.376039					
Mean of diagonals: 0.8752078					
Minimal of diagonals: 0.5796					

kernel functions, such as Gaussian, von Mises and Epanechnikov, with $S_0 = 500, S_c = 0, P_c = P_0 = 0.6$. The results are similar as shown by the high ARI values in Table 12. For S_0 , since it is the minimal size of a cluster to be recognized as a meaningful one, results won't change as long as S_0 is less than the minimal size of the clusters that we get. For P_0 , we get the same result for any P_0 within (0.6, 0.75).

3.6 Results from TRDG and MVCA

Results from TRDG

In this section, we show the result of applying TRDG to alanine dipeptide. We follow the steps in [5]: (1) In clustering step, microstates are obtained by grid clustering (see Section 3.2); (2) Estimating the free energy of each microstates $F_i \sim -kT \ln(Z_i)$ [5], with Z_i being the number of times the system visited the microstate; (3) Estimating the energy barrier $F_{ij} \sim -kT \ln(Z_{ij})$ [5] between microstates, where Z_{ij} is the minimum cut between microstates found by using Gomory-Hu algorithm implemented in the function “gomory_hu_tree” from the Python package “igraph”¹; (4) Starting with the lowest energy barrier F_{ij} , we construct the disconnectivity graph by connecting successively microstates in order of increasing F_{ij} . This step clusters microstates by using hierarchical clustering with single linkage.

To better illustrate the behavior of TRDG on alanine dipeptide, we construct TRDG based on microstates from grids with different sizes, i.e, a 10×10 grid, a 20×20 grid and an 80×80 grid. Figure 7 shows the results. Figure 7(A) shows the benchmark clustering results [6] of microstates defined by a 10×10 grid. Note that ideally a 10×10 grid will give 100 clusters (microstates); however, some of them are empty, which result in 90 non-empty clusters (microstates) as shown in Figure 7(A). The numbers from 1 to 90 are the indexes of microstates, and their locations denote the centers of the corresponding microstates. Figure 7(B) shows the TRDG ² results based on microstates defined in Figure 7(A). As shown in Figure 7(B), TRDG correctly

¹<https://igraph.org/python/>

²The disconnectivity graph is plotted by using the package “disconnectionDPS” downloaded from <http://www-wales.ch.cam.ac.uk/software.html>

Table 10: Transition matrix between clusters of Alanine dipeptide obtained by Gibbs'

	S0	S1	S2	S3	S4
S0	0.2867	0.1629	0.2686	0.2242	0.0576
S1	0.0048	0.9417	0.0037	0.0013	0.0486
S2	0.0256	0.0112	0.9497	0.0115	0.0019
S3	0.3437	0.0608	0.1761	0.3414	0.0780
S4	0.0021	0.0609	0.0008	0.0017	0.9345
Sum of diagonals: 3.4540					
Mean of diagonals: 0.6908					
Minimal of diagonals: 0.2867					

Table 11: Transition matrix between clusters of Alanine dipeptide obtained by Gibbs''

	S0	S1	S2	S3	S4	S5	S6
S0	0.9258	0.0055	0.0045	0.0030	0.0035	0.0562	0.0015
S1	0.0015	0.9337	0.0021	0.0010	0.0607	0.0008	0.0003
S2	0.1087	0.2027	0.2510	0.1638	0.0792	0.1329	0.0617
S3	0.0502	0.0774	0.1363	0.2846	0.2388	0.0785	0.1341
S4	0.0008	0.0477	0.0007	0.0024	0.9418	0.0062	0.0004
S5	0.0670	0.0044	0.0072	0.0054	0.0416	0.8740	0.0004
S6	0.0182	0.0166	0.0363	0.0979	0.0269	0.0047	0.7994
Sum of diagonals: 5.0102							
Mean of diagonals: 0.7157							
Minimal of diagonals: 0.2510							

84 recognized the microstates 31, 83, 75 and 72 as local stable states. However, microstates 72 and 83 should
85 not be clustered separately since they are actually from the same cluster S1. In addition, we represent the
86 TRDG results in Figure 7(B) as a phylogenetic tree shown in Figure 7(C), which contains the same clustering
87 structure as the one in (B), and is easier to read with the label coloring. As shown in Figure 7(C), TRDG
88 does not perform well on this dataset in terms of clustering, since the benchmark clusters are mixed up.
89 Figure 7(D) and Figure 7(E) shows the TRDG results based on microstates defined by a 20×20 grid and an
90 80×80 grid, respectively. Since we care more about the performance of TRDG on clustering, we only show
91 the phylogenetic tree representation of the TRDG for presenting clearly the cluster structure. By refining the
92 microstates, the clustering structure from TRDG is not improved as shown in Figure 7(D & E).
93 Note that we compare different methods based on microstates defined by an 80×80 grid. According to
94 the results in SI Figure 7(E) and Figure 4 in the main paper, TRDG did not performance well in terms of
95 clustering.

96

97 Results from MVCA

98 In this section, we show the result of applying TRDG to alanine dipeptide. We follow the steps in [7]: (1) using
99 symmetric Jensen-Shannon divergence to measure the similarity between microstates; (2) using agglomerative
100 clustering with Wards minimum variance criterion to cluster microstates into macrostates (metastable states),
101 and cutting the hierarchical clustering tree to give 6 clusters. The results are show in Figure 8.

102

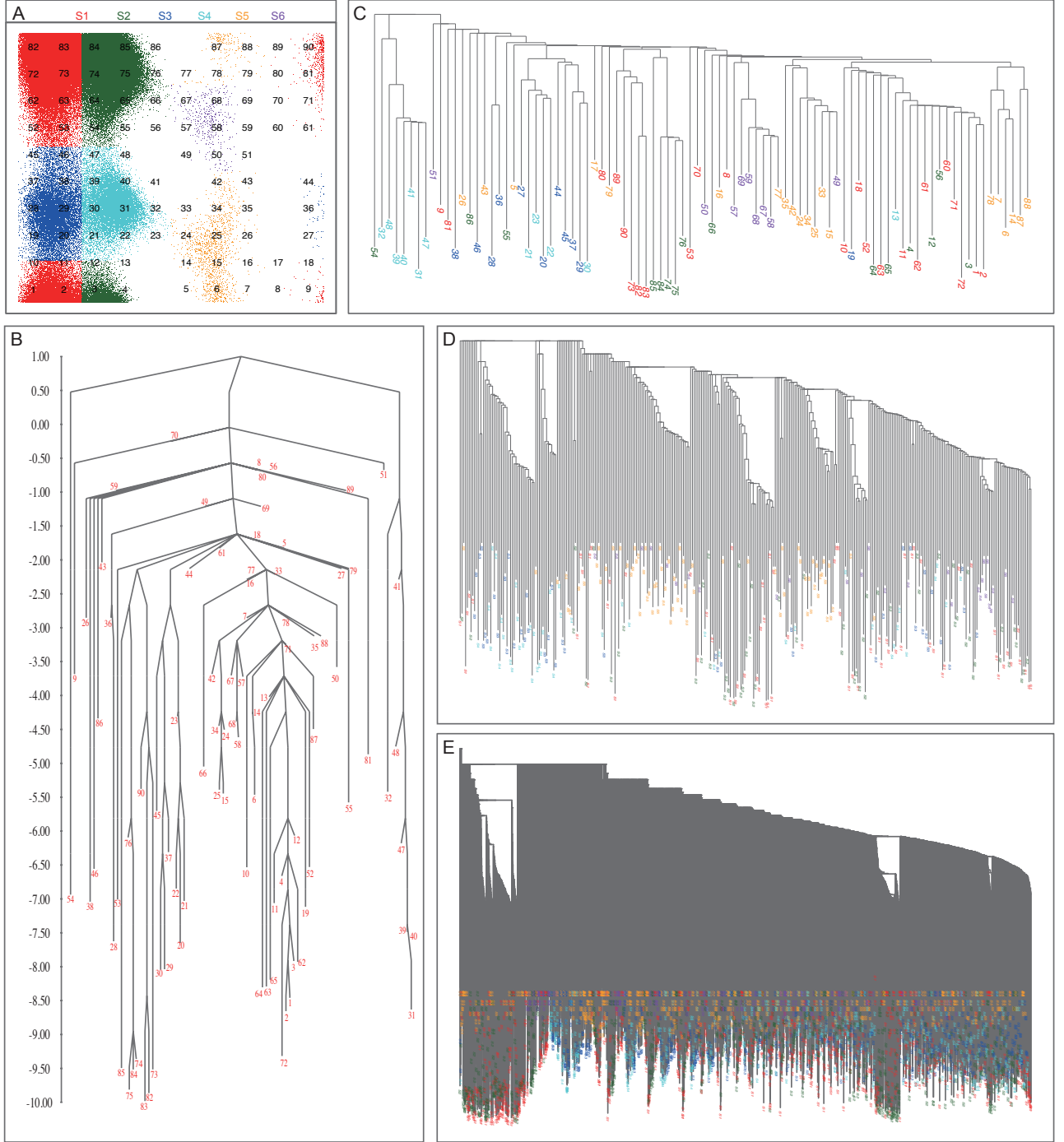


Figure 7: Transition disconnectivity graph (TRDG) of alanine dipeptide. The y-axis for (B-E) shows the free energy from low to high. (A) A 10×10 grid generates 90 non-empty microstates from 6 benchmark clusters (S1-S6) with cluster color code at the top. The numbers located at the center of each microstate are the indexes of microstates. (B) TRDG results with microstates defined by (A). The label of each node corresponds to the index of the microstate in (A). (C) Phylogenetic tree representation of the TRDG results in (B). It contains the same information in (B), but with extra coloring for the labels. The label of each node corresponds to the index of the microstate in (A). The color of labels corresponds to the cluster color in (A). (D) Phylogenetic tree representation of the TRDG for microstates defined by a 20×20 grid. The color of labels corresponds to the cluster color in (A). (E) Phylogenetic tree representation of the TRDG for microstates defined by an 80×80 grid. The color of labels corresponds to the cluster color in (A).

Table 12: ARI between cluster labels resulted from different kernel functions for analyzing Alanine dipeptide

ARI	von Mises	Epanechnikov
Gaussian	0.995622	0.9953416
Epanechnikov	0.9909818	-

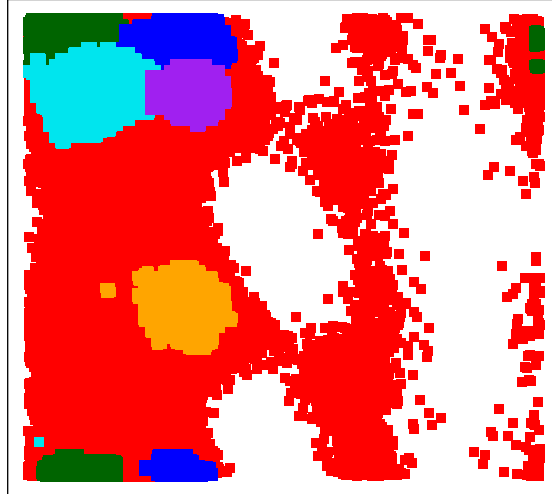


Figure 8: Clustering results of alanine dipeptide from MVCA. Different colors present different clusters.

103 4 Details about analyzing HP35 Nle/Nle

104 4.1 The value of d_0

105 We applied CAPT on the MD data of HP35 Nle/Nle by using $P_0 = 0.7, P_c = 0.95, S_0 = 500, S_c = 10000$,
 106 and the Gaussian kernel. The partition tree is shown in Figure 9. We then tried 5 different values for d_0 to
 107 compute the LDc and LDa values for the obtained clusters. Results are given in Table 13. We find that the
 108 order of the maximal LDc of these clusters do not vary with d_0 . However, the stable structure, i.e., the frame
 109 with maximal LDc in each cluster, may vary with d_0 , as shown in Figure 10. In the figure, the structures
 110 with the same color in each row are exactly the same frame. The MAD between the center of C39 under case
 111 B and case C is 0.1727754; The center of each cluster does not vary with d_0 , when $d_0 \leq 0.1972243$, and we
 112 set $d_0 = 0.1757350$.

113

114

115 4.2 Comparison with MPP

116 LDs of clusters obtained by MPP ³ are given in Table 14. Corresponding structures with the maximal LDc
 117 in each cluster are given in Figure 11. We find that the LDc's of cluster U and N2 are 67 and 8 respectively
 118 when $d_0 = 0.1757350$, which are smaller than the 6-th most stable cluster found by CAPT (LDc=763).

119

³The clustering labels are provided by the authors of [3]

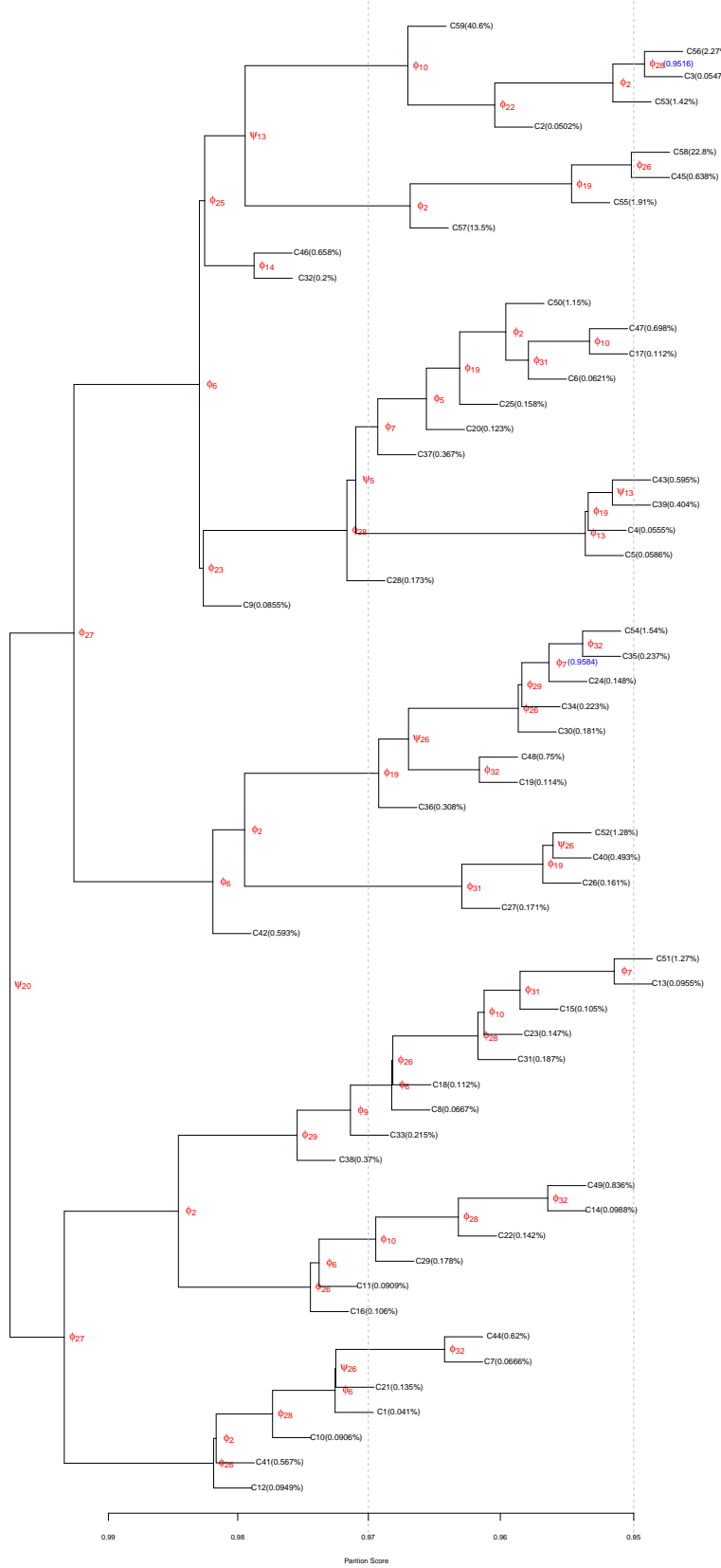


Figure 9: Partition tree of HP35 Nle/Nle, with $S_0 = 500$, $P_0 = 0.7$, $S_c = 10000$, $P_c = 0.95$ and the Gaussian kernel.

Table 13: The maximal local density LDc&LDa of each CAPT cluster calculated using different d_0 . ST stands for similarity threshold, Q. is the short for quantile.

ST Q.	$d_0 = 0.3418513$ (50%)		$d_0 = 0.2318932$ (5%)		$d_0 = 0.1972243$ (0.5%)		$d_0 = 0.1757350$ (0.05%)		$d_0 = 0.1594225$ (0.005%)	
	LDc	LDa	LDc	LDa	LDc	LDa	LDc	LDa	LDc	LDa
C1	12	12	3	3	2	2	1	1	1	1
C2	46	46	3	3	1	1	1	1	1	1
C3	67	67	4	4	1	1	1	1	1	1
C4	22	23	2	2	1	1	1	1	1	1
C5	24	24	3	3	1	1	1	1	1	1
C6	36	36	4	4	1	1	1	1	1	1
C7	33	33	3	3	2	2	1	1	1	1
C8	48	48	4	4	1	1	1	1	1	1
C9	180	220	42	42	6	6	3	3	1	1
C10	22	22	2	2	2	2	1	1	1	1
C11	15	15	3	3	1	1	1	1	1	1
C12	28	28	3	3	2	2	1	1	1	1
C13	23	23	7	7	2	2	1	1	1	1
C14	19	19	3	3	1	1	1	1	1	1
C15	46	46	3	3	1	1	1	1	1	1
C16	35	35	5	5	2	2	2	2	1	1
C17	552	1322	61	66	12	12	2	2	1	1
C18	46	50	6	6	1	1	1	1	1	1
C19	31	32	6	6	1	1	1	1	1	1
C20	80	80	12	12	3	3	1	1	1	1
C21	103	103	22	22	4	4	1	1	1	1
C22	37	50	5	5	2	2	1	1	1	1
C23	47	47	4	4	2	2	1	1	1	1
C24	69	69	7	7	2	2	2	2	1	1
C25	89	92	16	16	3	3	1	1	1	1
C26	62	62	3	3	1	1	1	1	1	1
C27	79	79	6	6	2	2	1	1	1	1
C28	104	104	38	38	4	4	2	2	1	1
C29	41	43	4	4	2	2	1	1	1	1
C30	180	180	10	10	2	2	1	1	1	1
C31	44	46	6	6	2	2	1	1	1	1
C32	87	87	5	5	1	1	1	1	1	1
C33	88	88	11	11	3	3	2	2	1	1
C34	28	30	4	4	2	2	1	1	1	1
C35	34	36	6	6	2	2	1	1	1	1
C36	29	29	3	3	1	1	1	1	1	1
C37	230	5977	25	25	5	5	3	3	1	1
C38	63	63	4	4	2	2	1	1	1	1
C39	2225	74916	627	638	126	126	21	21	4	4
C40	126	144	10	10	3	3	1	1	1	1
C41	113	121	10	10	3	3	1	1	1	1
C42	66	66	7	7	2	2	1	1	1	1
C43	109	109	9	9	3	3	2	2	1	1
C44	59	59	9	9	2	2	2	2	1	1
C45	45	46	6	6	2	2	1	1	1	1
C46	140	140	40	40	4	4	2	2	1	1
C47	184	135321	23	1228	5	20	2	2	1	1
C48	197	200	23	23	6	6	2	2	1	1
C49	88	89	8	8	2	2	1	1	1	1
C50	325	140438	20	20	5	5	2	2	1	1
C51	167	169	12	12	3	3	2	2	1	1
C52	158	180	21	21	6	6	2	2	1	1
C53	4283	7914	554	573	83	83	14	14	3	3
C54	90	118	8	9	2	2	1	1	1	1
C55	104	208	34	34	11	11	3	3	2	2
C56	5504	6852	554	554	110	110	20	20	4	4
C57	1719	2734	62	63	7	7	2	2	1	1
C58	4735	14087	118	118	38	38	14	14	4	4
C59	306331	307503	86021	86022	28297	28299	6854	6854	1303	1303

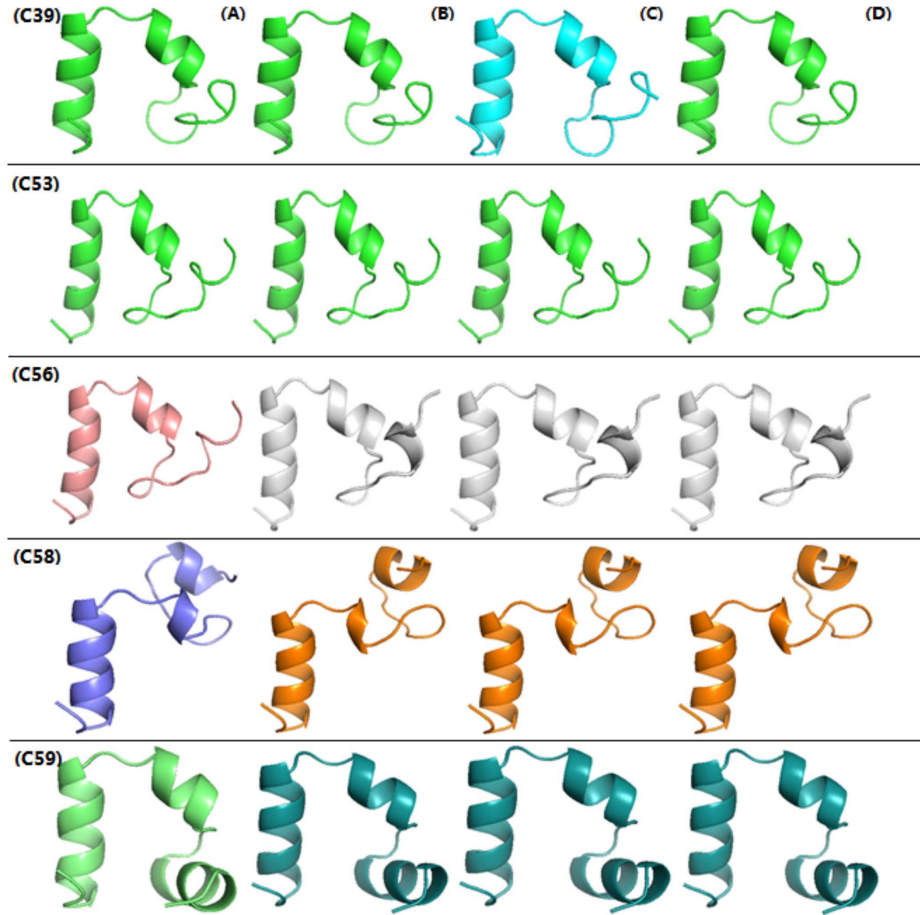


Figure 10: Different stable structures resulting from different d_0 by CAPT. Each column corresponds to different d_0 : (A) $d_0 = 0.2318932$; (B) $d_0 = 0.1972243$; (C) $d_0 = 0.1757350$; (D) $d_0 = 0.1594225$. The MAD between the centers of C39 under Case B and Case C is 0.1727754. The structures with the same color in each row are exactly the same frame.

Table 14: The maximal local density LDc&LDa of each MPP cluster calculated using different d_0 . ST stands for similarity threshold, Q. is the short for quantile.

ST Q.	$d_0 = 0.3418513$ (50%)		$d_0 = 0.2318932$ (5%)		$d_0 = 0.1972243$ (0.5%)		$d_0 = 0.1757350$ (0.05%)		$d_0 = 0.1594225$ (0.005%)	
	LDc	LDa	LDc	LDa	LDc	LDa	LDc	LDa	LDc	LDa
I1	114766	307002	71943	82447	27375	28299	6766	6854	1293	1303
N1	111358	294150	55576	58818	15659	15726	3789	3790	737	737
U	10134	119336	1978	2223	376	379	67	67	12	12
I2	84735	297628	20080	31423	4356	4759	816	839	130	133
N2	10647	44064	499	535	49	49	8	8	3	3

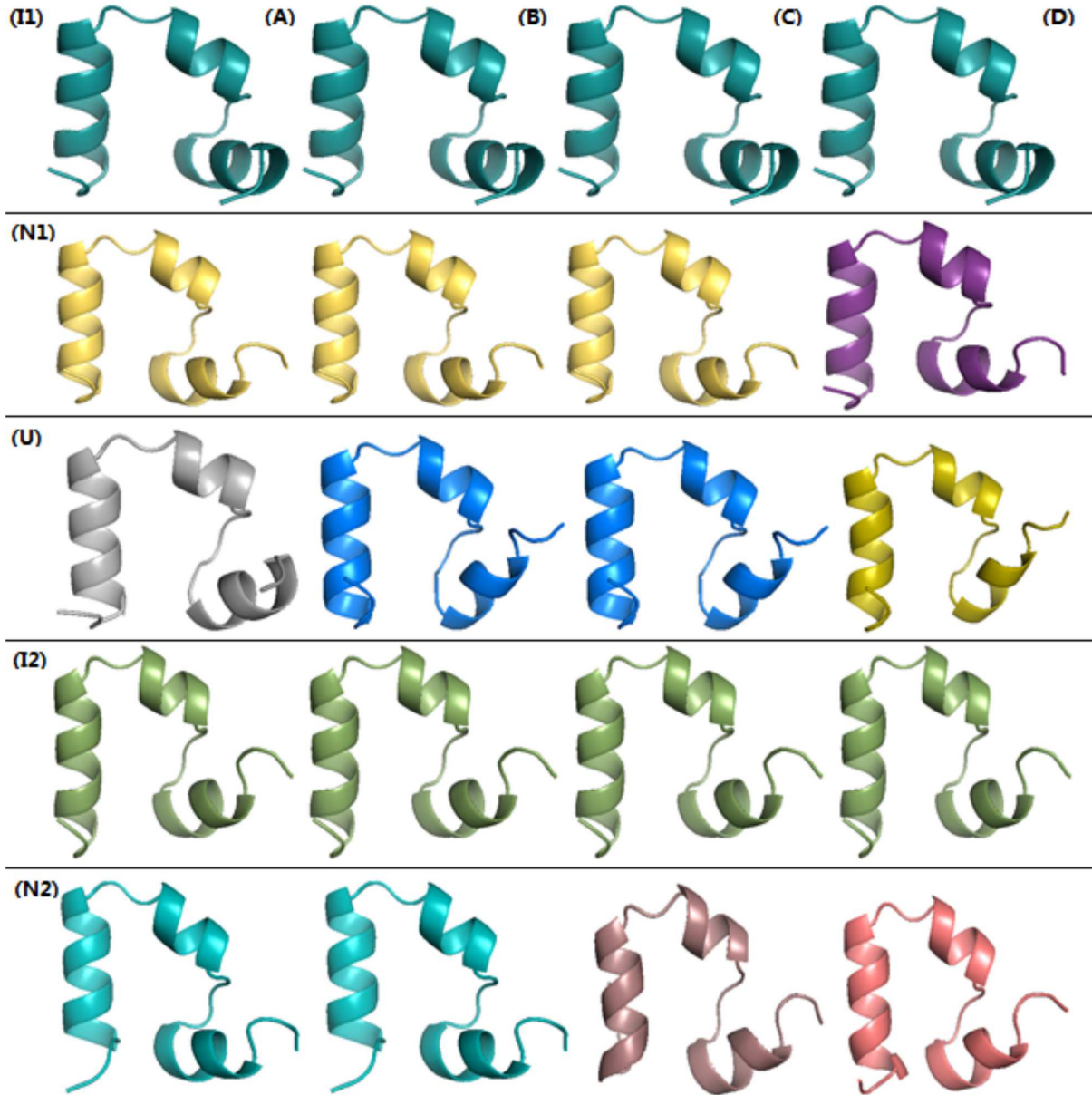


Figure 11: Different stable structures resulting from different d_0 by MPP. MPP found five clusters: I1, I2, U, N1 and N2. Each column corresponds to different d_0 : (A) $d_0 = 0.2318932$; (B) $d_0 = 0.1972243$; (C) $d_0 = 0.1757350$; (D) $d_0 = 0.1594225$. Detailed values of LDC and LDA are given in Table 14. The structures with the same color in each row are exactly the same frame.

120 **4.3 Sensitivity analysis**

121 In this part, we conduct the sensitivity analysis for the parameters S_0 and P_0 , as well as the kernel function for
 122 density estimation. S_0 , as discussed before, only determines the minimal size of each cluster we obtained. We
 123 set $S_0 = 10000$ for previous experiments. Here we also give the results while using $S_0 = 500$ with $P_0 = 0.7$ and
 124 the Gaussian kernel. Since there are many clusters, we first set $P_c = 0.95$. The results are given in Table 13
 125 and the partition tree is shown in Figure 9. These results show that there is only one stable cluster C59 with
 126 LDc=6854. We then set $P_c = 0.7$ and run CAPT on C59. The partition tree is shown in Figure 13, where we
 127 find 6 stable clusters, as shown in Table 15. These are exactly the same results found by setting $S_0 = 10000$.
 128 However, with a too large S_0 , we can not get the right number of clusters. Taking Alanine dipeptide as an
 129 example, we only get 4 clusters if we set $S_0 = 1948$ (i.e., 1% of the whole population), because there are
 130 only 1529 and 425 frames in the clusters S5 and S6 of Figure 4(A) in the main paper, respectively. So if one
 131 wants to explore the whole cluster structure, one should set a smaller value for S_0 , say, $100 \leq S_0 \leq 500$. For
 132 complex biomolecules, one may be interested only in the stable structures, and a larger value for S_0 seems
 133 more efficient in such cases.

Table 15: LDc of HP35 Nle/Nle clusters in the partition tree shown in Figure 13. d_0 is set as 0.1757350.

Cluster	L1	L2	L3	L4	L5	L6	L7	L8	L9
LDc	1	1	1	2	1	1	1	8	1
Cluster	L10	L11	L12	L13	L14	L15	L16	L17	L18
LDc	1	3	2	1	1	14	2	1	2
Cluster	L19	L20	L21	L22	L23	L24	L25	L26	L27
LDc	1	1	1	1	1	5	1	1	1
Cluster	L28	L29	L30	L31	L32	L33	L34	L35	L36
LDc	2	1	1	1	22	7	1	1	3
Cluster	L37	L38	L39	L40	L41	L42	L43	L44	L45
LDc	1	3	2	2	1	2	1	3	1
Cluster	L46	L47	L48	L49	L50	L51	L52	L53	L54
LDc	2	1	2	1	1	2	1	2	7
Cluster	L55	L56	L57	L58	L59	L60	L61	L62	L63
LDc	2	4	1	2	11	7	11	1	2
Cluster	L64	L65	L66	L67	L68	L69	L70	L71	L72
LDc	2	4	2	5	8	3	2	5	4
Cluster	L73	L74	L75	L76	L77	L78	L79	L80	L81
LDc	2	2	10	20	5	2	2	3	3
Cluster	L82	L83	L84	L85	L86	L87	L88	L89	L90
LDc	8	2	67	3	51	12	3167	1321	763
Cluster	L91	L92	L93						
LDc	834	3662	6854						

133

134 For P_0 , we tried five different values $\{0.6, 0.65, 0.7, 0.75, 0.8\}$, with $S_0 = 10000$ and the Gaussian kernel.
 135 The resulting partition trees are given in Figure 14, Figure 15, Figure 16, Figure 17 and Figure 18. The
 136 corresponding LDc values are given in Table 17, Table 18, Table 19, Table 20 and Table 21. A summary of
 137 stable clusters is given in Table 22. There are only 5 stable clusters when $P_0 = 0.8$. For $0.6 \leq P_0 \leq 0.75$, we
 138 get 6 stable clusters. Interestingly, although the resulting partition trees are different for different values of
 139 P_0 , the key energy barriers between these 6 stable clusters are the same.

140 For the kernel function used for density estimation, we tried three different kernels: Gaussian, von Mises and
 141 Epanechnikov. They result in the same stable clusters, as shown in Table 23 and Table 24. Note that for
 142 different kernel functions, the partition trees are a bit different, as shown in Figure 19 and Figure 20. In
 143 addition, we show the ARI values between cluster labels from different kernel functions in Figure 12. As we
 144 can see from the figure, ARI is sensitive to the partition score cutoff, which is reasonable. Different kernel
 145 functions result in density estimates of different smoothness. ARI may drop at some cutoff, however it will be
 146 pulled up later as shown in the figure. For example, when cutoff=0.82, ARI(G,V)> 0.99; however, it drops

Table 16: Transition Matrix between meaningful clusters obtained by CAPT for HP35 Nle/Nle. 'Other' are conformations not belonging to S1-S6.

	other	S1	S2	S3	S4	S5	S6
other	0.9886	0.0003	0.0033	0.0007	0.0027	0.0002	0.0041
S1	0.0101	0.9230	0.0006	0.0062	0.0000	0.0600	0.0001
S2	0.0662	0.0004	0.9199	0.0000	0.0090	0.0000	0.0046
S3	0.0111	0.0040	0.0000	0.9099	0.0005	0.0736	0.0009
S4	0.0551	0.0000	0.0093	0.0008	0.8826	0.0001	0.0520
S5	0.0067	0.0641	0.0000	0.1430	0.0003	0.7827	0.0032
S6	0.0361	0.0000	0.0020	0.0004	0.0223	0.0009	0.9383

¹⁴⁷ to 0.9 when cutoff=0.81, and goes to 0.96 when cutoff=0.8. Even for the same angle, the partition scores are
¹⁴⁸ different under different kernel functions. That is, from a local point of view, the result is sensitive to the
¹⁴⁹ kernel function; however, from a global point of view, it is insensitive to the kernel function.

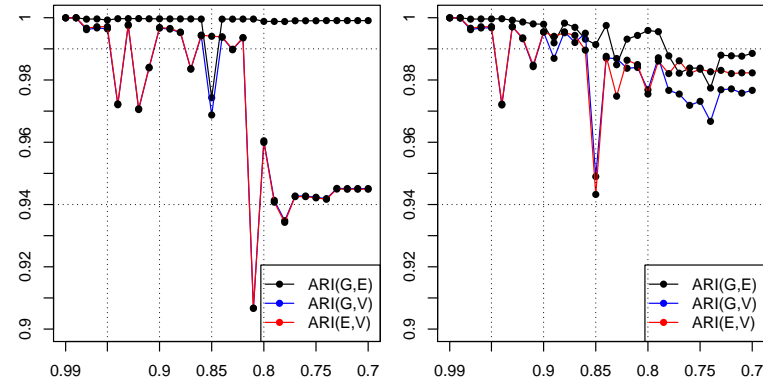


Figure 12: ARI between cluster labels based on different kernel functions under different value of S_0 with $S_c = 10000$, $P_c = P_0 = 0.7$. The left panel is for the case $S_0 = 10000$, and the right panel is for the case $S_0 = 500$. In the figure, the x-axis is the energy barrier and the y-axis is the ARI. ARI(E,V) is the ARI between cluster labels based on the Epanechnikov kernel and the von Mises kernel, ARI(G,E) is the ARI between cluster labels based on the Gaussian kernel and the Epanechnikov kernel, ARI(G,V) is the ARI between cluster labels based on the Gaussian kernel and the von Mises kernel.

Table 17: LDc with $d_0 = 0.1757350$ of centers of HP35 Nle/Nle in partition tree shown in Figure 14

Cluster	L1	L2	L3	L4	L5	L6	L7	L8	L9
LDc	2	1	2	3	2	2	2	1	12
Cluster	L10	L11	L12	L13	L14	L15	L16	L17	L18
LDc	1	14	4	2	3	2	1	2	2
Cluster	L19	L20	L21	L22	L23	L24	L25	L26	L27
LDc	1	2	3	51	2	2	1	2	1
Cluster	L28	L29	L30	L31	L32	L33	L34	L35	L36
LDc	2	8	2	2	1	2	1	1	1
Cluster	L37	L38	L39	L40	L41	L42	L43	L44	L45
LDc	4	1	1	2	2	1	2	2	2
Cluster	L46	L47	L48	L49	L50	L51	L52	L53	L54
LDc	1	2	2	22	2	3	2	2	1
Cluster	L55	L56	L57	L58	L59	L60	L61	L62	L63
LDc	2	3	5	3	3	8	2	2	2
Cluster	L64	L65	L66	L67	L68	L69	L70	L71	L72
LDc	1	2	2	4	3	2	2	2	3
Cluster	L73	L74	L75	L76	L77	L78	L79	L80	L81
LDc	21	2	2	14	20	2	2	2	2
Cluster	L82	L83	L84	L85	L86	L87	L88	L89	
LDc	3	1	1321	3167	834	763	3663	6854	

Table 18: LDc with $d_0 = 0.1757350$ of centers of HP35 Nle/Nle in the partition tree shown in Figure 15

Cluster	L1	L2	L3	L4	L5	L6	L7	L8	L9
LDc	3	2	2	2	1	14	4	1	14
Cluster	L10	L11	L12	L13	L14	L15	L16	L17	L18
LDc	2	3	2	1	2	2	2	2	1
Cluster	L19	L20	L21	L22	L23	L24	L25	L26	L27
LDc	2	3	51	2	1	1	2	2	2
Cluster	L28	L29	L30	L31	L32	L33	L34	L35	L36
LDc	2	2	2	8	3	2	2	2	4
Cluster	L37	L38	L39	L40	L41	L42	L43	L44	L45
LDc	1	1	2	2	2	1	2	2	2
Cluster	L46	L47	L48	L49	L50	L51	L52	L53	L54
LDc	1	2	2	1	1	2	2	3	1
Cluster	L55	L56	L57	L58	L59	L60	L61	L62	L63
LDc	3	2	3	1	2	1	2	2	2
Cluster	L64	L65	L66	L67	L68	L69	L70	L71	L72
LDc	2	2	4	3	3	1	5	3	2
Cluster	L73	L74	L75	L76	L77	L78	L79	L80	L81
LDc	21	2	2	2	2	2	20	1	2
Cluster	L82	L83	L84	L85	L86	L87	L88		
LDc	12	1321	3167	834	763	3663	6854		

Table 19: LDc with $d_0 = 0.1757350$ of centers of HP35 Nle/Nle in the partition tree shown in Figure 16

Cluster	L1	L2	L3	L4	L5	L6	L7	L8	L9
LDc	1	2	1	2	2	2	14	4	1
Cluster	L10	L11	L12	L13	L14	L15	L16	L17	L18
LDc	3	2	2	2	14	2	3	51	1
Cluster	L19	L20	L21	L22	L23	L24	L25	L26	L27
LDc	1	1	2	8	2	2	2	2	2
Cluster	L28	L29	L30	L31	L32	L33	L34	L35	L36
LDc	2	2	2	4	1	1	2	2	2
Cluster	L37	L38	L39	L40	L41	L42	L43	L44	L45
LDc	1	3	2	1	2	2	1	2	3
Cluster	L46	L47	L48	L49	L50	L51	L52	L53	L54
LDc	2	1	2	2	3	1	2	2	1
Cluster	L55	L56	L57	L58	L59	L60	L61	L62	L63
LDc	2	2	2	2	4	3	2	1	5
Cluster	L64	L65	L66	L67	L68	L69	L70	L71	L72
LDc	1	2	21	3	1	2	2	2	2
Cluster	L73	L74	L75	L76	L77	L78	L79	L80	L81
LDc	2	20	2	2	2	3	12	1321	3167
Cluster	L82	L83	L84	L85					
LDc	834	763	3663	6854					

Table 20: LDc with $d_0 = 0.1757350$ of centers of HP35 Nle/Nle in the partition tree shown in Figure 17

Cluster	L1	L2	L3	L4	L5	L6	L7	L8	L9
LDc	1	2	1	2	51	2	14	1	3
Cluster	L10	L11	L12	L13	L14	L15	L16	L17	L18
LDc	2	2	14	2	2	1	1	1	2
Cluster	L19	L20	L21	L22	L23	L24	L25	L26	L27
LDc	8	2	2	2	2	2	2	2	1
Cluster	L28	L29	L30	L31	L32	L33	L34	L35	L36
LDc	1	2	2	2	1	3	2	1	2
Cluster	L37	L38	L39	L40	L41	L42	L43	L44	L45
LDc	2	1	2	3	2	1	2	3	1
Cluster	L46	L47	L48	L49	L50	L51	L52	L53	L54
LDc	2	2	2	3	1	2	2	2	4
Cluster	L55	L56	L57	L58	L59	L60	L61	L62	L63
LDc	2	2	2	1	1	2	21	3	1
Cluster	L64	L65	L66	L67	L68	L69	L70	L71	L72
LDc	2	4	5	2	2	2	20	2	2
Cluster	L73	L74	L75	L76	L77	L78	L79	L80	L81
LDc	2	2	5	3	12	1321	3167	834	763
Cluster	L82	L83							
LDc	3666	6854							

Table 21: LDc with $d_0 = 0.1757350$ of centers of HP35 Nle/Nle in the partition tree shown in Figure 18

Cluster	L1	L2	L3	L4	L5	L6	L7	L8	L9
LDc	1	2	1	14	2	2	2	2	21
Cluster	L10	L11	L12	L13	L14	L15	L16	L17	L18
LDc	2	2	1	1	2	2	2	2	3
Cluster	L19	L20	L21	L22	L23	L24	L25	L26	L27
LDc	1	1	1	2	2	1	4	2	3
Cluster	L28	L29	L30	L31	L32	L33	L34	L35	L36
LDc	3	2	2	1	3	1	2	1	2
Cluster	L37	L38	L39	L40	L41	L42	L43	L44	L45
LDc	2	2	3	2	1	2	3	2	2
Cluster	L46	L47	L48	L49	L50	L51	L52	L53	L54
LDc	3	2	2	4	20	2	2	2	1
Cluster	L55	L56	L57	L58	L59	L60	L61	L62	L63
LDc	14	1	3	2	2	2	3	2	5
Cluster	L64	L65	L66	L67	L68	L69	L70	L71	L72
LDc	2	2	12	3167	2	763	834	3764	6854

Table 22: clusters with maximal LDc (Top 6) under different P_0 , where S1-6 is the cluster name used to give a unified comparison. Corresponding structure is given in Figure 6.

		S1	S2	S3	S4	S5	S6
$P_0 = 0.8$	cluster	L67	L69	L71	L70	-	L72
	LDc	3167	763	3764	834	-	6854
$P_0 = 0.75$	cluster	L79	L81	L82	L80	L78	L83
	LDc	3167	763	3666	834	1321	6854
$P_0 = 0.7$	cluster	L81	L83	L84	L82	L80	L85
	LDc	3167	763	3663	834	1321	6854
$P_0 = 0.65$	cluster	L84	L86	L87	L85	L83	L88
	LDc	3167	763	3663	834	1321	6854
$P_0 = 0.6$	cluster	L85	L87	L88	L86	L84	L89
	LDc	3167	763	3663	834	1321	6854

Table 23: LDc with $d_0 = 0.1757350$ of centers of HP35 Nle/Nle in the partition tree shown in Figure 19

Cluster	L1	L2	L3	L4	L5	L6	L7	L8	L9
LDc	1	2	1	2	2	2	14	4	1
Cluster	L10	L11	L12	L13	L14	L15	L16	L17	L18
LDc	2	3	2	2	2	14	51	3	1
Cluster	L19	L20	L21	L22	L23	L24	L25	L26	L27
LDc	1	1	2	8	2	2	2	2	2
Cluster	L28	L29	L30	L31	L32	L33	L34	L35	L36
LDc	2	2	2	4	1	1	2	2	2
Cluster	L37	L38	L39	L40	L41	L42	L43	L44	L45
LDc	1	3	2	1	2	2	1	2	3
Cluster	L46	L47	L48	L49	L50	L51	L52	L53	L54
LDc	2	1	2	2	3	1	2	2	1
Cluster	L55	L56	L57	L58	L59	L60	L61	L62	L63
LDc	2	2	2	2	4	3	2	1	5
Cluster	L64	L65	L66	L67	L68	L69	L70	L71	L72
LDc	1	2	21	3	1	2	2	2	2
Cluster	L73	L74	L75	L76	L77	L78	L79	L80	L81
LDc	2	20	2	2	2	3	12	1321	3167
Cluster	L82	L83	L84	L85					
LDc	834	763	3663	6854					

151 5 Remark on the von Mises kernel

Assuming that $\{\theta_i, i = 1, \dots, n\}$ follows $vM(\mu, \kappa)$, the density estimate using a standard von Mises kernel [8] is given by

$$\hat{f}(\theta, v) = \frac{1}{n(2\pi)I_0(v)} \sum_{i=1}^n e^{v \cos(\theta - \theta_i)}, \quad (1)$$

where

$$v = \left\{ \frac{3n\hat{\kappa}^2 I_2(2\hat{\kappa})}{4\sqrt{\pi}I_0(\hat{\kappa})^2} \right\}^{\frac{2}{5}}, \quad (2)$$

152 $\hat{\kappa}$ is the MLE of κ , $I_r(v)$ is the modified Bessel function of order r , and v takes the role of (inverse of)
153 smoothing parameter. In practice, the computer gives $I_0(v) = \infty$ when $v > 709$, i.e., larger than the maximal
154 number that the computer can handle with. Thus we set $v = 709$ when v is actually bigger than 709 in
155 analysis.

Table 24: LDc with $d_0 = 0.1757350$ of centers of HP35 Nle/Nle in the partition tree shown in Figure 20

Cluster	L1	L2	L3	L4	L5	L6	L7	L8	L9
LDc	1	1	2	2	1	2	4	1	14
Cluster	L10	L11	L12	L13	L14	L15	L16	L17	L18
LDc	2	2	3	2	1	14	2	5	1
Cluster	L19	L20	L21	L22	L23	L24	L25	L26	L27
LDc	3	2	2	1	2	2	1	8	2
Cluster	L28	L29	L30	L31	L32	L33	L34	L35	L36
LDc	2	1	2	2	2	4	1	2	2
Cluster	L37	L38	L39	L40	L41	L42	L43	L44	L45
LDc	2	3	1	2	2	2	1	2	2
Cluster	L46	L47	L48	L49	L50	L51	L52	L53	L54
LDc	3	2	1	2	1	2	3	2	2
Cluster	L55	L56	L57	L58	L59	L60	L61	L62	L63
LDc	51	1	2	2	2	4	2	2	3
Cluster	L64	L65	L66	L67	L68	L69	L70	L71	L72
LDc	1	5	1	21	3	2	1	2	2
Cluster	L73	L74	L75	L76	L77	L78	L79	L80	L81
LDc	2	2	2	2	2	12	20	2	3
Cluster	L82	L83	L84	L85	L86	L87			
LDc	1321	3167	834	3662	763	6854			

¹⁵⁶ **6 Partition trees of HP35 Nle/Nle under different settings**

¹⁵⁷

¹⁵⁸

¹⁵⁹

¹⁶⁰

¹⁶¹

¹⁶²

¹⁶³

¹⁶⁴

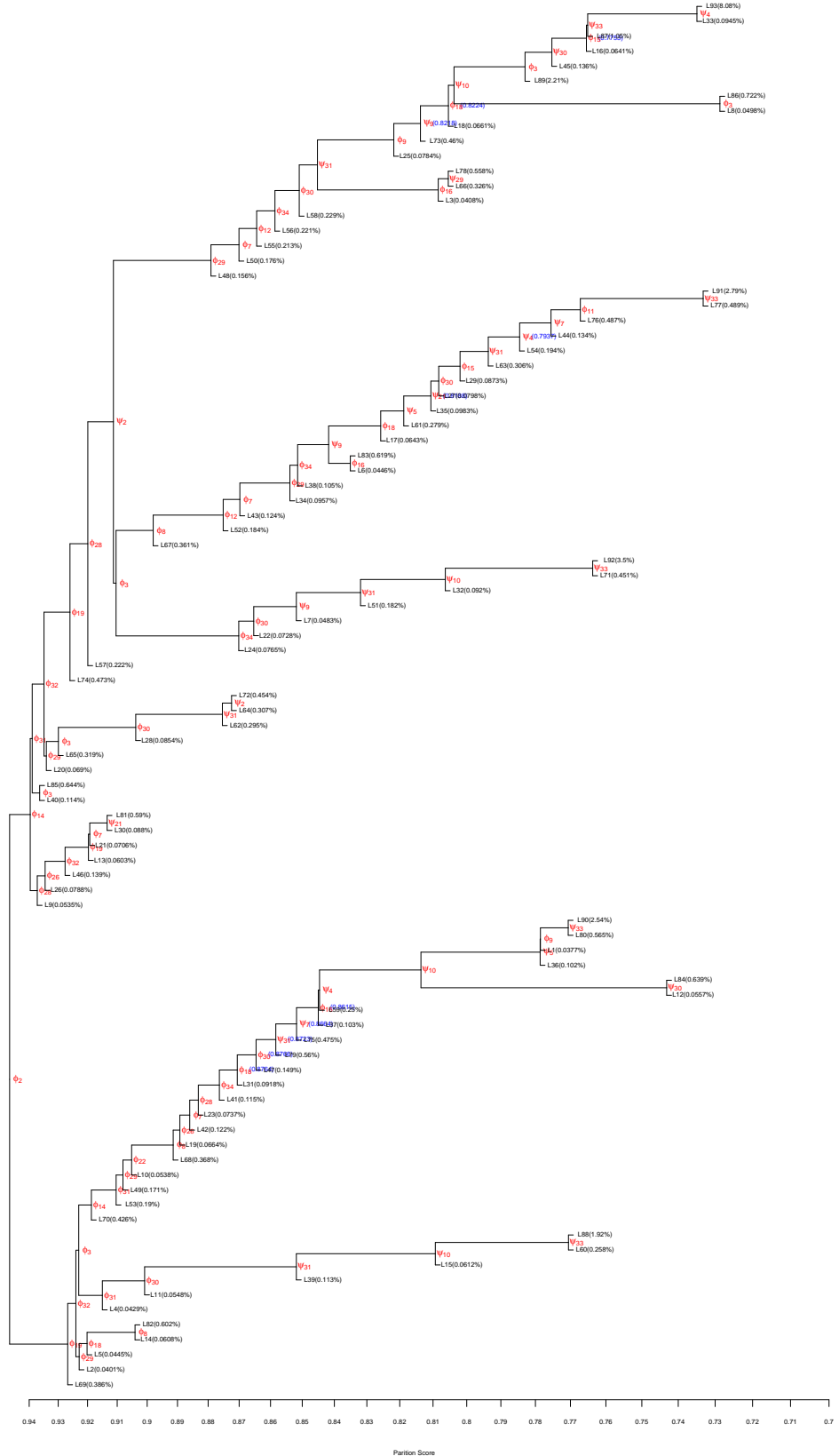


Figure 13: Sub-partition tree of C59 in Figure 9 for HP35 Nle/Nle with $S_0 = 500$, $P_c = P_0 = 0.7$, and the Gaussian kernel. In the tree, the root node is C59.

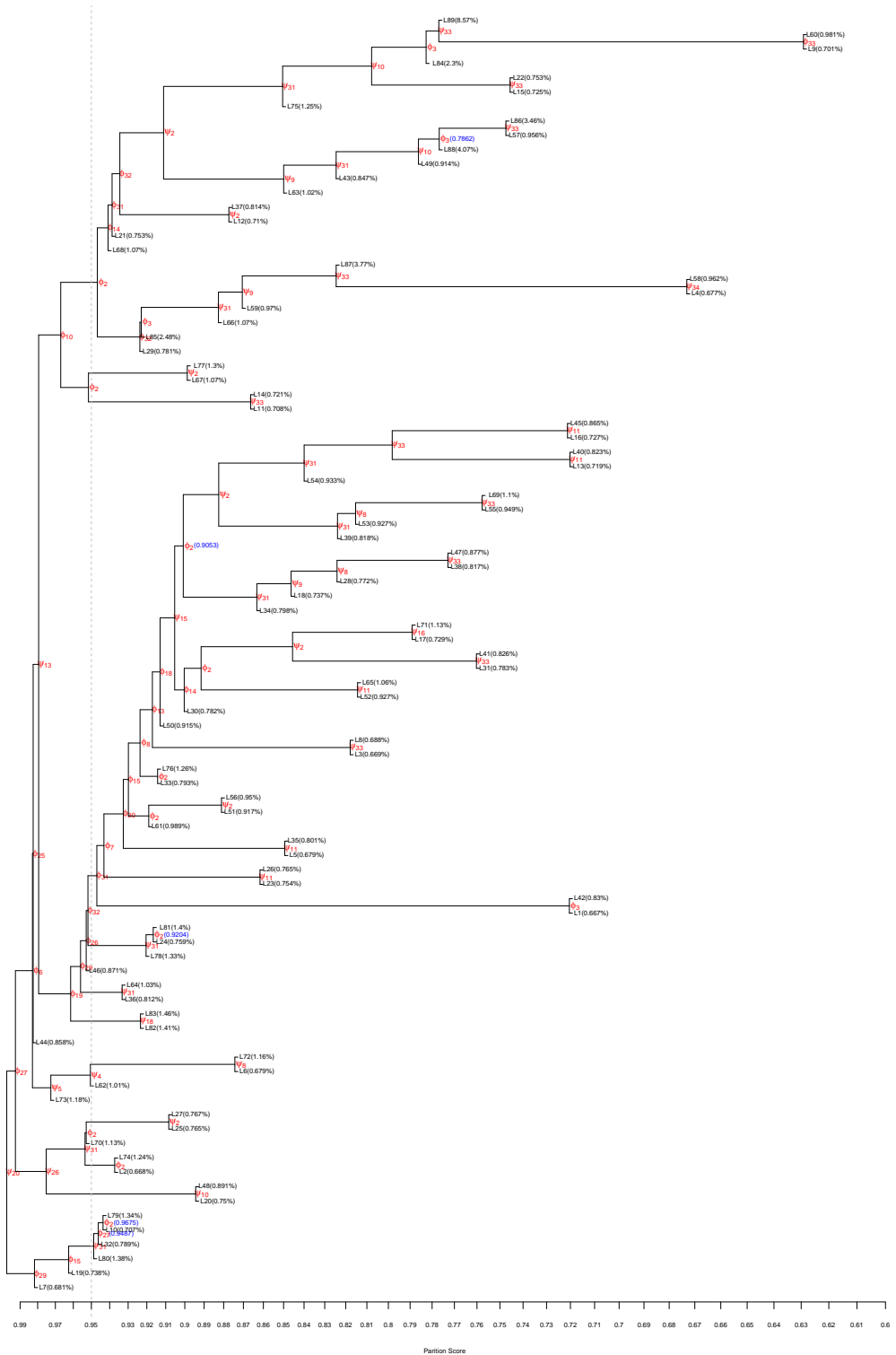


Figure 14: Partition tree of HP35 Nle/Nle with $S_0 = 10000$, $P_c = P_0 = 0.6$, and the Gaussian kernel.

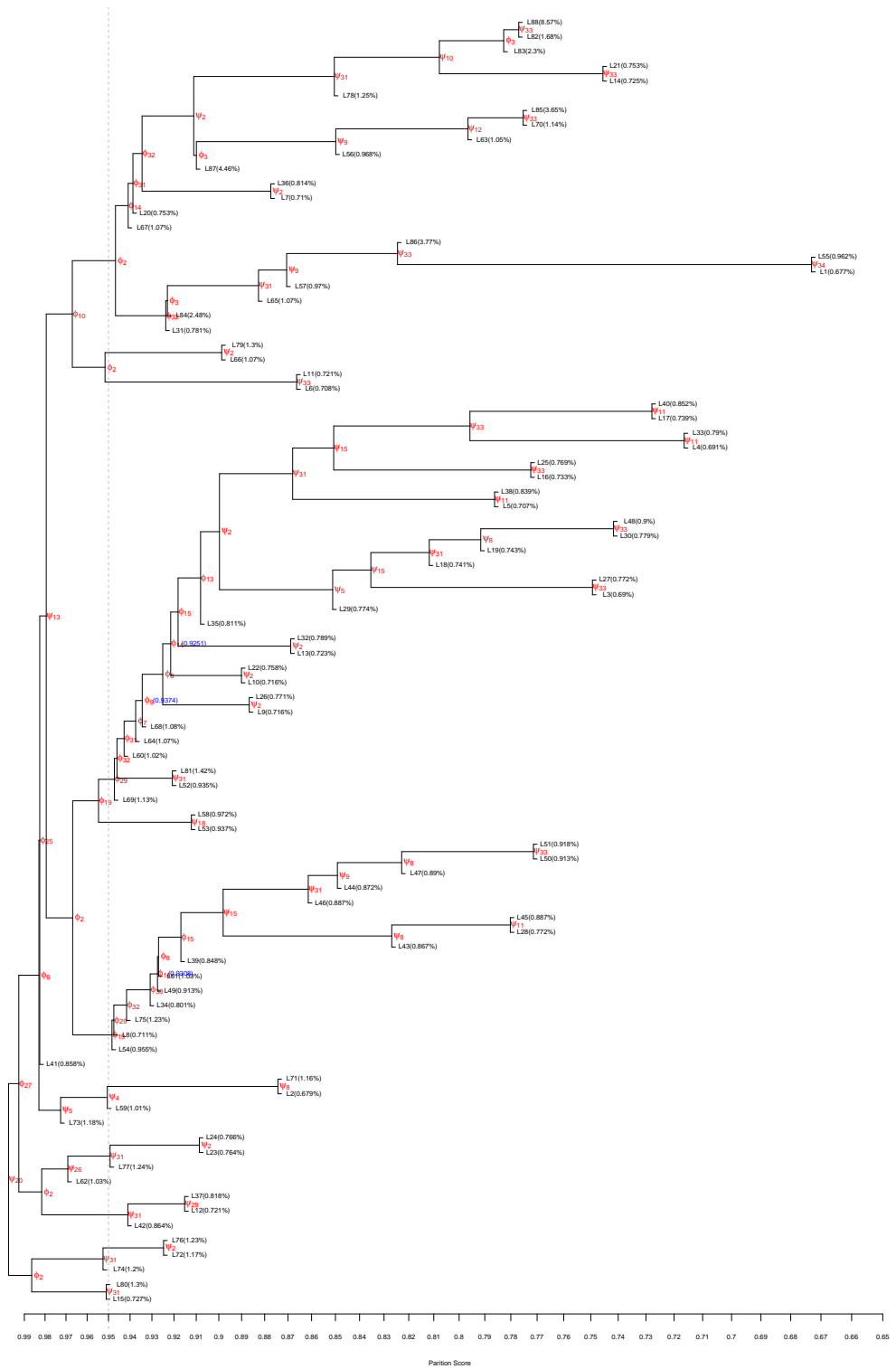


Figure 15: Partition tree of HP35 Nle/Nle with $S_0 = 10000$, $P_c = P_0 = 0.65$, and the Gaussian kernel.

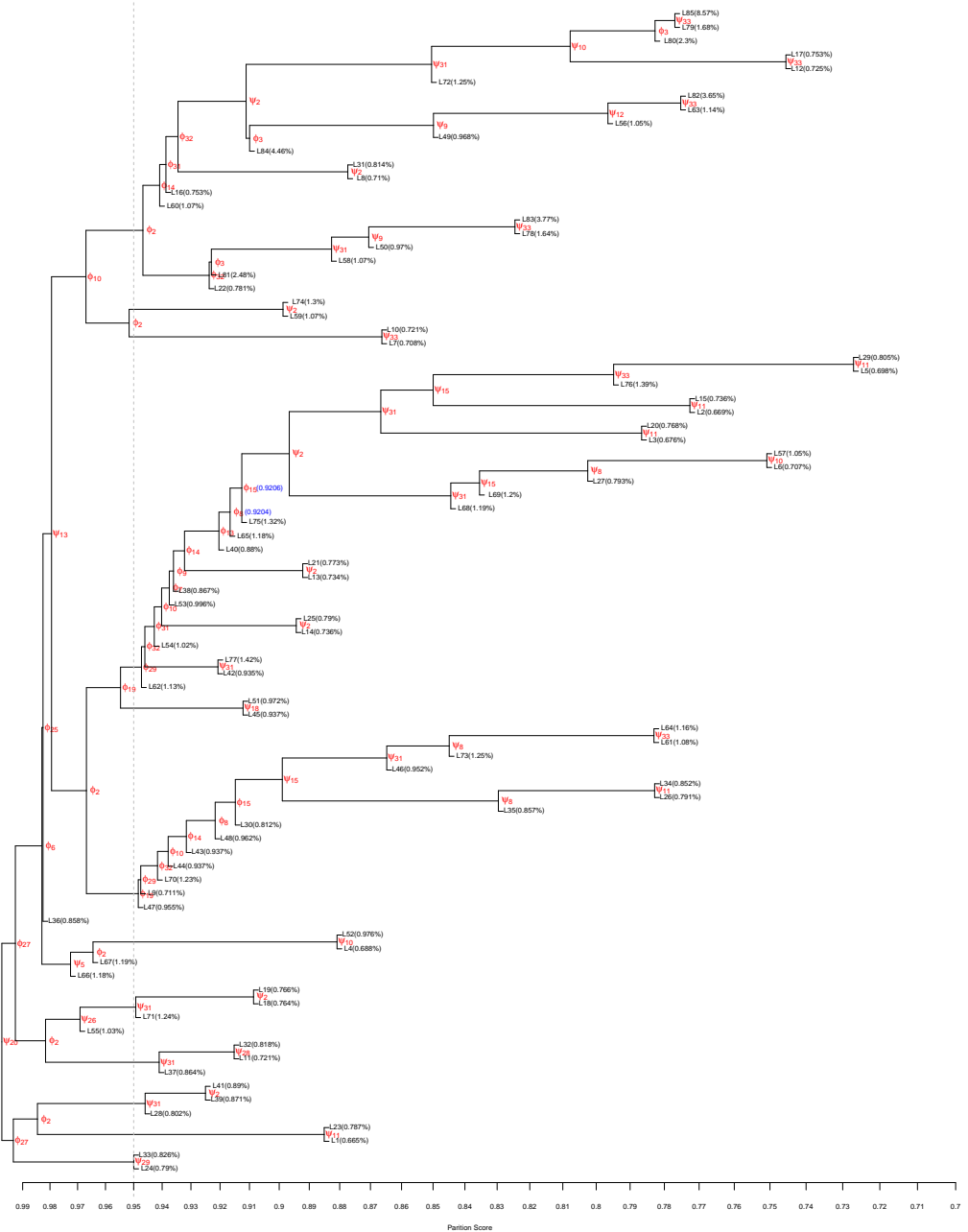


Figure 16: Partition tree of HP35 Nle/Nle with $S_0 = 10000$, $P_c = P_0 = 0.7$, and the Gaussian kernel.

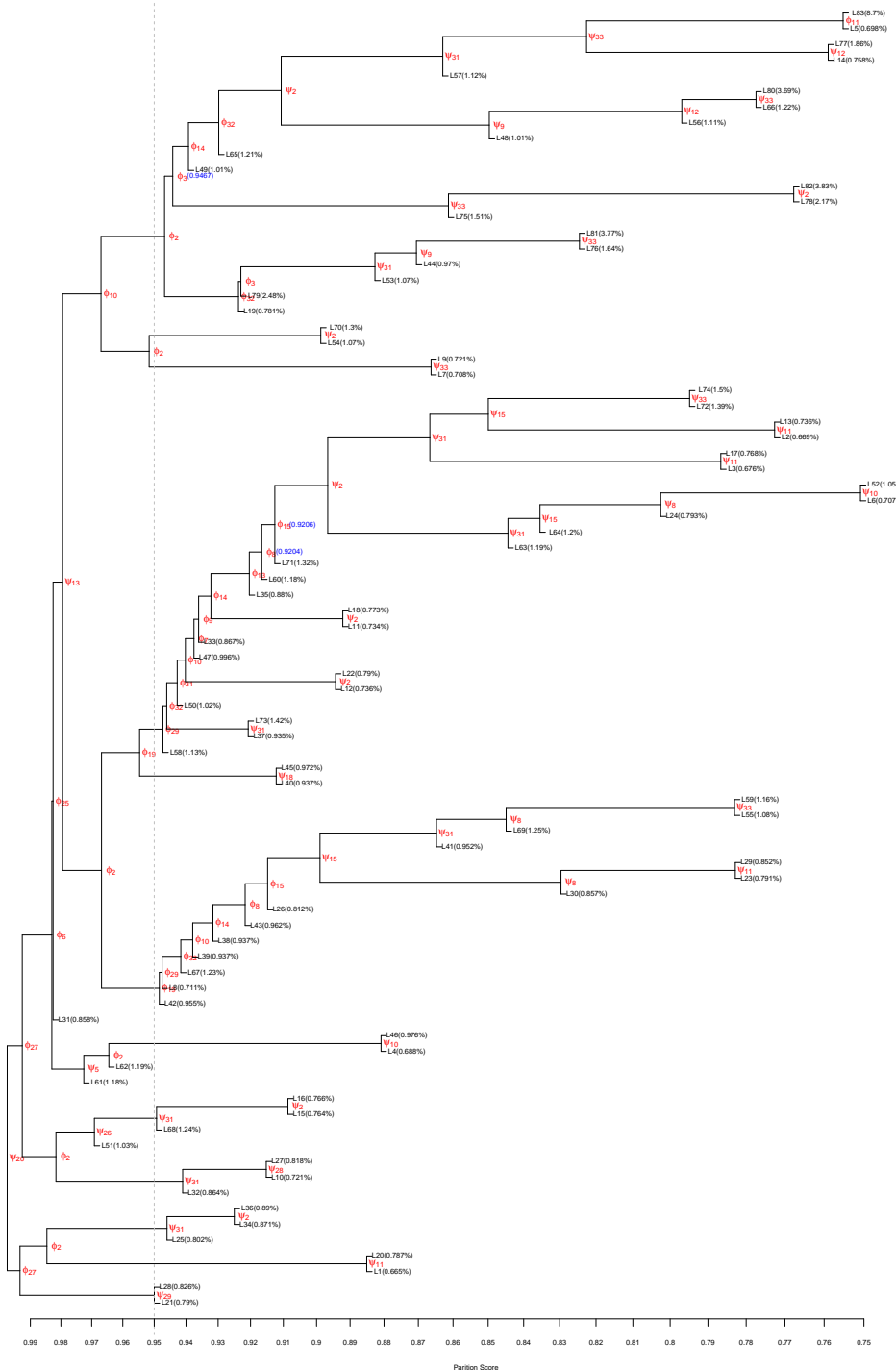


Figure 17: Partition tree of HP35 Nle/Nle with $S_0 = 10000$, $P_c = P_0 = 0.75$, and the Gaussian kernel.

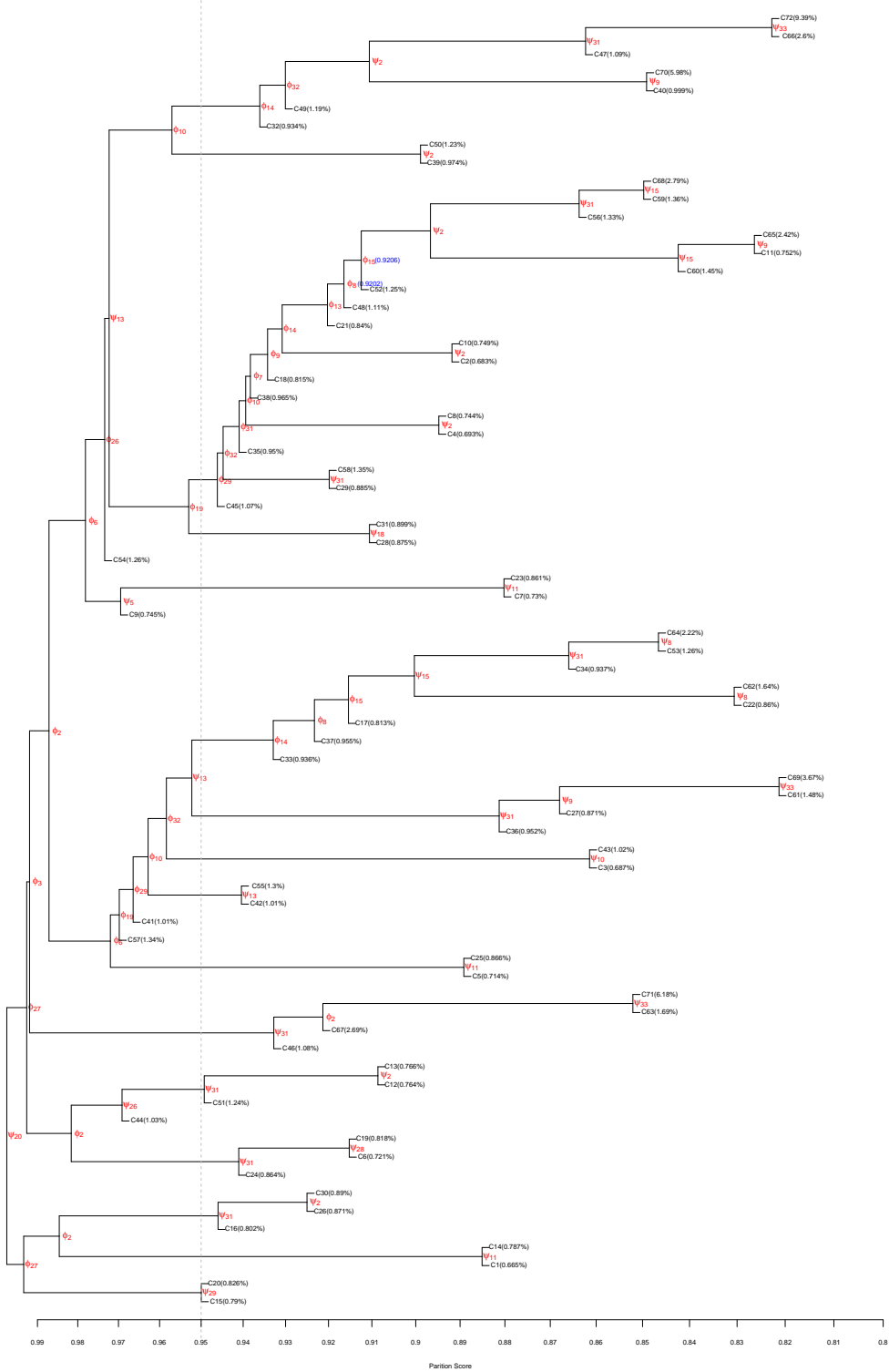


Figure 18: Partition tree of HP35 Nle/Nle with $S_0 = 10000$, $P_c = P_0 = 0.8$, and the Gaussian kernel.

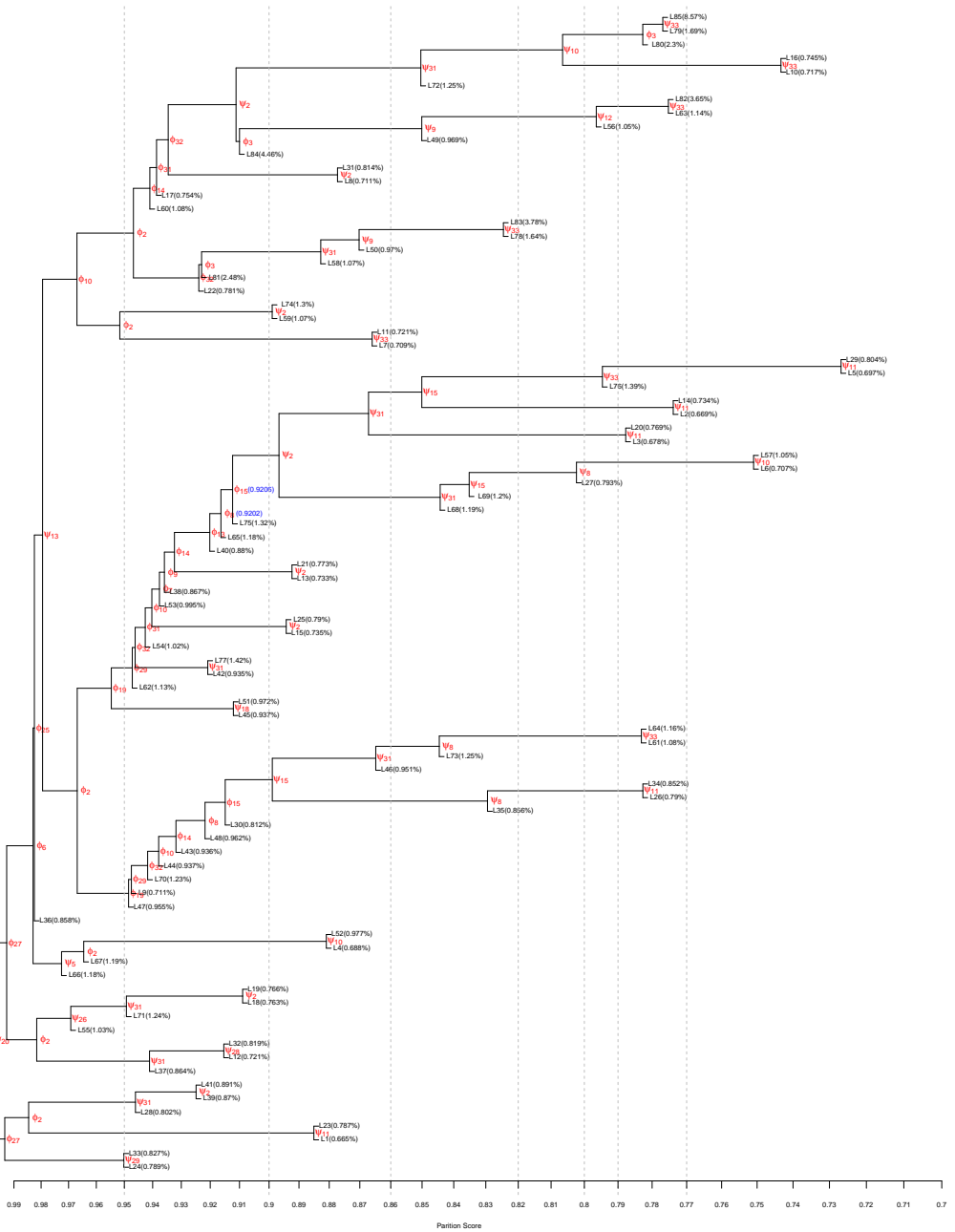


Figure 19: Partition tree of HP35 Nle/Nle with $S_0 = 10000$, $P_c = P_0 = 0.7$, and the Epanechnikov kernel.

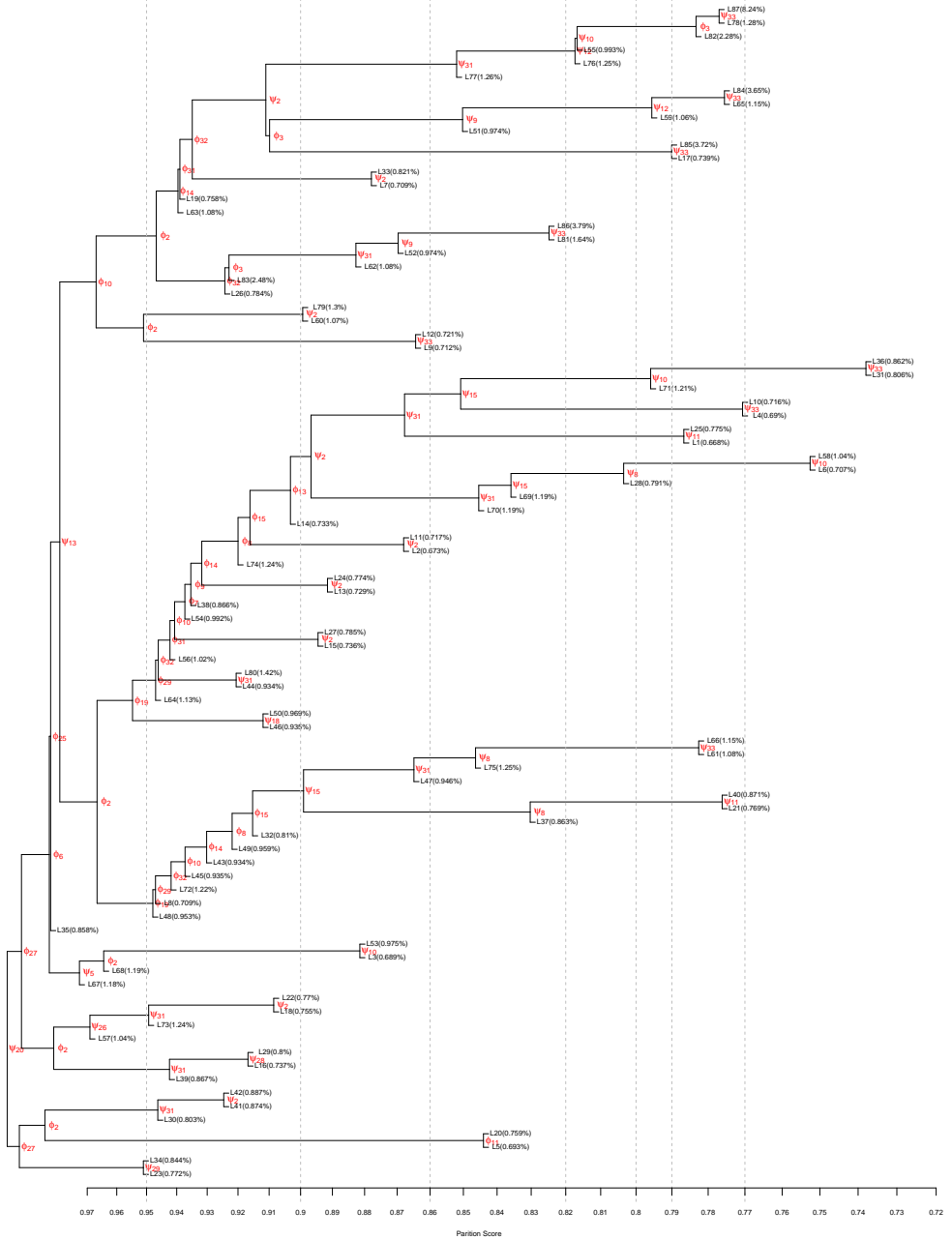


Figure 20: Partition tree of HP35 Nle/Nle with $S_0 = 10000$, $P_c = P_0 = 0.7$, and the von Mises kernel.

₁₆₅ **References**

- ₁₆₆ [1] Lars Skjærven, Xin-Qiu Yao, Guido Scarabelli, and Barry J Grant. Integrating protein structural dynamics
₁₆₇ and evolutionary analysis with bio3d. *BMC bioinformatics*, 15(1):399, 2014.
- ₁₆₈ [2] Alexandros Altis, Phuong H Nguyen, Rainer Hegger, and Gerhard Stock. Dihedral angle principal
₁₆₉ component analysis of molecular dynamics simulations. *The Journal of Chemical Physics*, 126(24):244111,
₁₇₀ 2007.
- ₁₇₁ [3] Abhinav Jain and Gerhard Stock. Hierarchical folding free energy landscape of HP35 revealed by most
₁₇₂ probable path clustering. *The Journal of Physical Chemistry B*, 118(28):7750–7760, 2014.
- ₁₇₃ [4] Yuguang Mu, Phuong H Nguyen, and Gerhard Stock. Energy landscape of a small peptide revealed by
₁₇₄ dihedral angle principal component analysis. *Proteins: Structure, Function, and Bioinformatics*, 58(1):45–
₁₇₅ 52, 2005.
- ₁₇₆ [5] Sergei V Krivov and Martin Karplus. Hidden complexity of free energy surfaces for peptide (protein)
₁₇₇ folding. *Proceedings of the National Academy of Sciences*, 101(41):14766–14770, 2004.
- ₁₇₈ [6] John D Chodera, William C Swope, Jed W Pitera, and Ken A Dill. Long-time protein folding dynamics
₁₇₉ from short-time molecular dynamics simulations. *Multiscale Modeling & Simulation*, 5(4):1214–1226, 2006.
- ₁₈₀ [7] Brooke E Husic, Keri A McKiernan, Hannah K Wayment-Steele, Mohammad M Sultan, and Vijay S
₁₈₁ Pande. A minimum variance clustering approach produces robust and interpretable coarse-grained models.
₁₈₂ *Journal of chemical theory and computation*, 14(2):1071–1082, 2018.
- ₁₈₃ [8] Charles C Taylor. Automatic bandwidth selection for circular density estimation. *Computational Statistics
184 & Data Analysis*, 52(7):3493–3500, 2008.